RSC Advances

ROYAL SOCIETY OF CHEMISTRY

www.rsc.org/advances

Journal Name

RSCPublishing

ARTICLE

Sisal-derived activated carbons for cost-effective lithium-sulfur batteries

Cite this: DOI: 10.1039/x0xx00000x

M. Raja, N. Angulakshmi[#], A. Manuel Stephan*

Received 00th January 2012,
Accepted 00th January 2012

DOI: 10.1039/x0xx00000x

www.rsc.org/

Elemental sulfur was successfully impregnated in an activated carbon (AC) matrix obtained from sisal fibers. The impregnation of sulfur in the activated carbon (S-AC) matrix was confirmed by XRD, SEM and Raman analyses. The sulfurized activated carbon (S-AC) composite electrode was employed as a cathode material for lithium- sulfur (Li-S) cell. The Li-S cell delivered a discharge capacity of **950** $mAhg^{-1}$ at 0.1C-rate. The electrochemical impedance spectroscopy measurements were carried out for the Li-S cell before and after cycling and also at different depth of discharge and depth of charge. A stable cycling was achieved at 1C-rate.

Introduction

Although lithium-ion batteries have been identified as a potential power source for portable electronic gadgets such as laptop computers, mobile phone, digital cameras etc., they cannot meet out the demands for hybrid electric vehicles and power grid applications[1,2]. Among the cathode materials for rechargeable lithium batteries explored so far, the elemental sulfur offers a highest theoretical capacity of 1672 mAh g^{-1} which is approximately ten times higher than that of lithium transition metal oxides or phosphates[3]. The unique properties such as low cost, widespread availability, better safety, wide operating temperature and long cycle life make lithium-sulfur batteries more attractive[4,5]. However, commercialization of lithium-sulfur batteries is hampered due to the poor electrical conductivity of sulfur ($5x10^{-30}$ S cm^{-1} at 25°C), formation, shuttling of higher-order polysulfides during charging and poor interfacial properties of lithium metal anode. Numerous review articles describe the working principle of Li-S batteries, the-state-of-art, advantages and their limitations[6-9]. Basically, sulfur cathode hosts two lithium-ions by dissimilation (non-topotactic) process and supports for the electrochemical redox reaction $16Li+ S_8 \rightarrow 8Li_2S$[6].

Although, Li-S battery system was introduced by Herbert and Ulam[10] in 1962, its technological importance was realized only in the beginning of year 2000. Different strategies have been made to enhance the electrical contact of sulfur by wrapping/ impregnating it with electrically conducting carbonaceous materials. The change in the volume of sulfur during cycling can be effectively controlled by cavities and porous structure. This pores/ cavities can also be used to absorb the polysulfides formed in situ during the cycling process[9].

Several methods were employed to prevent the formation and shuttling of polysulfides; for e.g. incorporation of electrolyte additives[11,12], metal oxide absorbents[13,14]. However, the performance of Li-S cells was not appreciable. In order to enhance electrical conductivity, sulfur particles were either coated with carbon precursor or wrapped by templates. Although macroporous carbons can store 60 wt.% of sulfur with its large pore volume, the electrochemical reactivity with Li^+- was found to be lower due to the poor electronic conductivity of composite cathode[15]. It is therefore, suggested that carbon with a combination mesoporous and microporous will be suitable for the applications in sulfur-carbon composite cathodes.

Manthiram and co-workers reported the cycling profile of sulfur -carbon nanocomposite cathode material comprising high surface area-black pearls. A stable cycling profile was achieved for a pluronic block co-polymer laden electrode material than the un-laden[16]. In a different approach, a flexible composite cathode films composed of CNT and sulfur was successfully employed by Jin et.al,[17] in a Li-S cell. The cell retained a discharge capacity of 740 mAh g^{-1} even after 100 cycles at 0.1 C. Attempts have also been made to improve the performance of Li-S batteries by coating

conducting polymer over carbon surface[18]. Very recently, Bruckner and co-workers demonstrated that the performance of Li-S cathode depends mainly on the amount of electrolyte, sulfur loading and C-rate. According to the authors excess of electrolyte, high rate and low loading of sulfur (approximately 40%) can significantly enhance the cycle life and capacity retention of Li-S batteries[19]. This work was further supported by Ye et al.,[20]. Also of importance, the electrolyte for Li-S cells plays a vital role in its performance. The formation of polysulfide reduction and their migration in subsequent cycling remains a problem area[21].

Although, the use of carbon as a matrix to wrap/encapsulate sulfur in order to increase its conductivity has been very exotic, the performance of Li-S cells is mainly influenced by nature of carbon, current density, amount of sulfur loaded and nature of the electrolyte.

In the recent past, activated carbons from biomass precursors have been introduced as electrode material for lithium-ion batteries due to their advantages such as inexpensive and waste management. The activated carbons obtained from biomass precursors such as sugar[22] peanut shells[23] cherry stones[24] were used as anode for lithium-ion batteries. One of the authors has employed coffee shells and banana fibers as biomass precursors as active materials for lithium-ion batteries and supercapacitors[25, 26]. However, the reports on sulfur impregnated activated carbons for applications in lithium-sulfur batteries are very scanty. Very recently, Moreno et al, [27] employed activated carbons derived from olive stones activated with KOH for lithium-sulfur batteries. In the recent years, several attempts have been made to address the issues of lithium batteries by identifying suitable cathodes and electrolytes[28-31].

In the present study, sisal fiber (botanical name Agave sisalane) was used as a carbon source for the first time due to its wide availability and low cost. It is widely cultivated in Brazil, Mexico and India. Although, the importance of sisal fiber is diminished (with competition from polypropylene), traditionally, sisal fiber was used as agricultural twine. In the recent years, sisal has been extensively used as a strengthening agent to replace asbestos and fiberglass and also in automobile industries. In the present work the activated carbon obtained from sisal carbon was used to encapsulate sulfur in order to prevent the pulverization of sulfur particles and to enhance their conductivity. Also of importance the electrochemical properties with a focus on electrochemical impedance spectroscopy (EIS) are discussed in order to produce cost-effective lithium-sulfur batteries.

Experimental

Pyrolysis of sisal fibre

High-quality sisal fibers were obtained from fields in Tamilnadu, India and were washed and dried. Finally whitish fibers were treated with concentrated solution of phosphoric acid (H_3PO_4) as porogen for 5 days at 35°C. The fiber:porogen ratio was 1:10 by weight. Pyrolysis was carried out under nitrogen atmosphere at 800°C at a heating ramp of 5°C min^{-1} for a period of 3 h. The obtained activated carbon was washed several times with de-ionized water until it reaches a pH value of 7.

Sulfurization of activated carbon

The sulfurized activated carbon (S-AC) was prepared by in-situ deposition from aqueous solution of sodium thiosulfate ($Na_2S_2O_3.5H_2O$) with the addition of hydrochloric acid as illustrated in Scheme 1. 10g of $Na_2S_2O_3.5H_2O$ was dissolved in 100 ml of de-ionized water and the solution was allowed for magnetic stirring for more than 12 h along with the activated carbon. The hydrochloric acid (0.5M) was slowly added to the solution in order to get sulfur precipitate according to the following reaction.

$S_2O_3^{2-}(Aq) \rightarrow S(s) + SO_3^{2-}(Aq)$ ---------- (1)

The sulfur was deposited in/and or on the surface of the activated carbon matrices. The solution was filtered and obtained sulfurized activated carbon (S-AC) was dried and kept at 80°C in an air oven for 12 h.

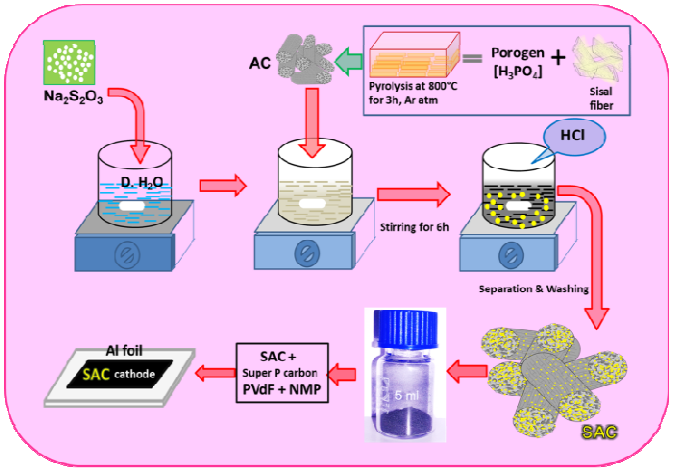

Scheme 1. Preparation method of sulfurized-activated carbon (SA-C).

Elemental analysis for the S-AC was done by an (Perkin-Elmer CHN 2000) elemental analyzer and the content of sulfur in the carbon matrix was around 60%. Powder X-ray diffraction patterns were recorded

between 10°and 80° (Jeol X-ray diffractometer, model, D/Max 2500) fitted with a nickel-filtered Cu-Kα radiation source. The morphologies of the pyrolytic carbons were examined by a (FESEM S-4700, Hitachi, Japan) scanning electron microscope. The histogram on the pore diameter of the activated carbon was measured using a software (Image J) as described by us earlier[32]. Thermo gravimetric analysis was conducted in the temperature range between 20-1000°C at a heating rate of 10°C/min in a N_2 atmosphere. The morphology and microstructure of the synthesized products were analyzed using high-resolution transmission electron microscopy (HR-TEM) of JEM-2100 at an acceleration voltage of 200 kV. Brunauer- Emmett- Teller (BET) surface area measurements were carried out using (Micrometrics ASAP2010) surface area analyzer. CHN analysis (ElementerVario EL III- Germany) was performed for the activated and sulfurized activated carbons. Raman spectra were recorded on a (RenishawinVia) spectrometer with He-Ne Laser at a wave length of 633 nm.

Electrochemical characterizations

Sulfur-activated carbon composite (S-AC) electrodes for charge-discharge studies were prepared by doctor blade-coating a slurry of 70 wt.% of the S-C, 10 wt.% of poly(vinylidene fluoride) and 20 wt.% Super P carbon dispersed in *N*-methyl-2-pyrrolydone on an aluminum foil, followed by drying at 100°C in an air oven, roller-pressing the dried sheets, and punching out circular sheets. The cyclic voltammetry (CV) curves were recorded (Solartron, UK) at a scan rate of 0.1 mV S^{-1} between 3 and 1.6 V.

A 2032-type coin cell was assembled with S-AC electrode and lithium metal foil (Foote Minerals) with an electrolyte comprising 1M $LiN(CF_3SO_2)_2$ in a 1:1 (v/v) mixture of 1,3 Dioxalane (1,3 DIOX) and tetraethylene glycol dimethylether (TEGDME) in an argon-filled glove box (M Braun, Germany). Galvanostatic charge–discharge profiles were made between 3 V and 1.5V by a computer-controlled battery testing unit (Arbin, USA). The electrochemical impedance spectroscopy (EIS) measurements were carried out (Biologic, France) before and after cycling and also for different depth of discharge (DOD) and depth of charge (DOC) of the Li-S cell. The values of R_{ct}, R_f and R_e were calculated by employing Z view software.

Results and Discussions

Carbonization of sisal and their properties

Figure 1 shows the thermo gravimetric traces of sisal fibers. The observed weight loss of about 2% around 90°C is attributed to the removal of moisture and further reduction in weight up to 200°C is due to the release of volatile[33]. At 205°C, hemi-cellulose starts to decompose with a corresponding weight loss of about 70%. Around 330°C the decomposed hemi-cellulose produce abundant organic compounds such as wood tar, methanol and ketone and were vaporized due to the absorbed heat. Finally, the carbonization starts around 515°C[34].

Generally, the heat generated during the decomposition of the porogen or any chemical reaction of the products of decomposition of the porogen with the fibers may alter the chemical composition of the carbonaceous products[35,36]. Porosity in carbonaceous materials can be generated by use of several chemical activation agents such as H_3PO_4, $AlCl_3$, $MgCl_2$, LiCl, Na_2CO_3, K_2CO_3, NaOH, KOH, and $ZnCl_2$. Although, numerous attempts have been made on chemical activation, the mechanism of the process is yet to be fully elucidated[37-41].

In the present study, the oxygen from the added-H_3PO_4 acid removes the cross-linking and stabilizes the carbon atoms in crystallites. During the pyrolysis process phosphate may intercalate and force apart the lamellae of the crystallites[42]. Removal of phosphate by, say, washing creates microporosity in the new structure[26,42]. Further, the surface area of the activated carbon is greatly varied due to the action of the porogens. For example, the BET surface area of AC is 234 m^2g^{-1} which is approximately six times (43 m^2g^{-1}) higher than that of un-treated. The microstructural evolutions can significantly influence the electrochemical behavior of the carbons.

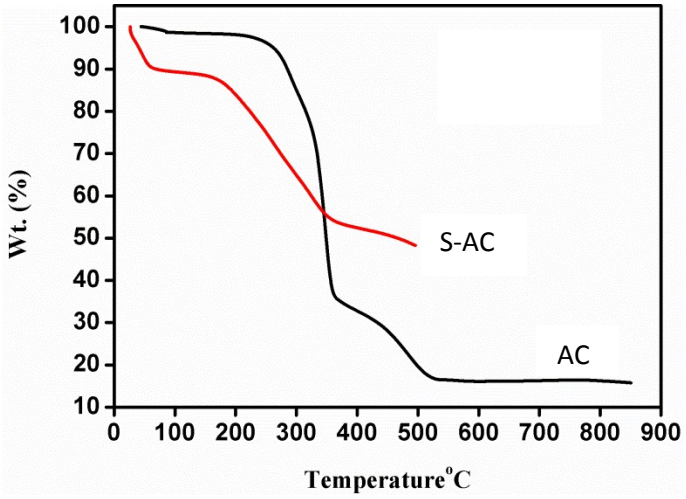

Figure.1. Thermal gravimetric traces of AC and S-AC

The nitrogen adsorption/desorption isotherm is depicted in Figure 2 which clearly indicates the type I nature of the activated carbon spheres of well-

developed mesopores. Also it is evident from Figure 2(b) the peak pore width of the activated carbon lies around 12Å. The BET surface area and content of carbon, sulfur, nitrogen and hydrogen for the activated and un-activated carbonaceous materials are depicted in Table 1.

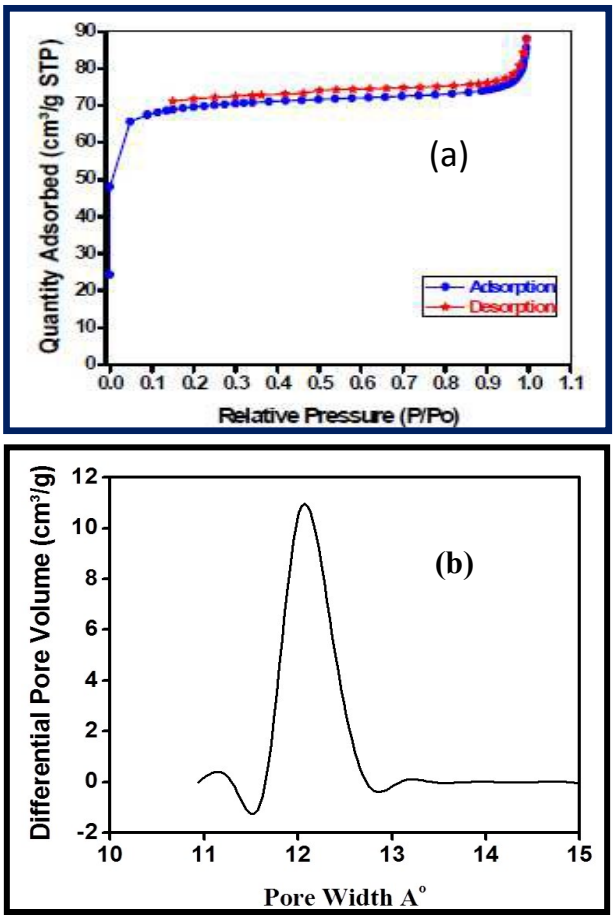

Figure.2(a) Adsorption/desorption curves of activated carbon. (b) Pore size distribution of activated carbon.

Table 1. CHN and BET surface area analyses

Type of Carbon	BET Surface area (m^2/g)	C (%)	H (%)	N (%)	Pore Volume cm^3g^{-1}
Untreated	43	64	2.1	0.16	16
Treated	818	40	1.4	0.07	24.5

Figure 3 (a) shows the XRD pattern of the sulfur impregnated activated carbon sample. The two peaks that appear at 24° and 43° (2θ) degrees are assigned to the (0 0 2) and (1 0 0) reflections respectively, which represents the crystallographic planes of the graphite. The peak around 43° represents honeycomb structures formed by sp2 hybridized carbons, while the broad (1 0 0) reflection at 24° (0 0 2) indicates small domains of coherent and parallel stacking of the graphene sheets[25, 42]. Interestingly, the sulfurized activated carbon (S-AC) exhibits (Figure 3 (a)) well-defined sulfur peaks and are assigned to the orthorhombic sulfur polymorph (JCPDS 00-008-0247).

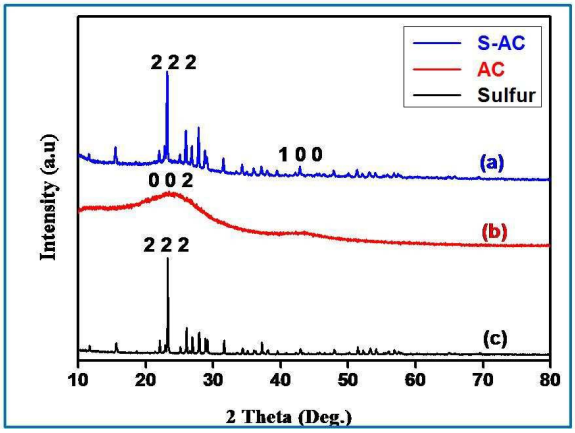

Figure:3 X-ray diffractograms of sulfurized activated carbon, activated carbon and sulfur

The high intensity peaks indicate that the activated carbon particles obtained from sisal fibers provide deposition sites for elemental sulfur, favoring an environment for precipitation[41]. These results are consistent with those reported earlier on carbon-sulfur composites irrespective of the carbon matrix employed[27].

Raman spectroscopy has been widely employed to identify carbonaceous materials and also to assess their graphitic content[44].

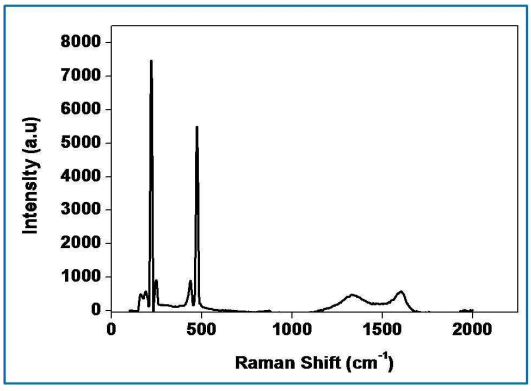

Figure 4. Raman spectrum of S-AC

It is clear from Figure 4 that the intensity of the D and G- Raman scattering peaks of activated carbon at 1350 and 1580 cm^{-1} represents respectively. The presence of sulfur peaks implies the impregnation of sulfur in the activated carbon matrix. The SEM images (Figure 5 (a&b)) reveal the morphology of the activated carbon and sulfurized activated carbon. The S-AC shows a bundle like structure with pores of various diameters that varies from 25–125 micrometers. The white feather like structure which appears on the surface of the carbon is attributed to the presence of ash and was easily removed by washing several times with de-ionized water[34]. The sulfurized activated carbon, on the other hand, shows a similar morphology partially filled with sulfur on the surface as well as into the pores. During the preparation process elemental sulfur is partially infiltrated into the carbon due to its adsorption properties and high surface area[27]. The TEM and elemental mapping of sulfur images (Figure 5 c & d) respectively confirms the coating and impregnation of sulfur in the carbon matrix.

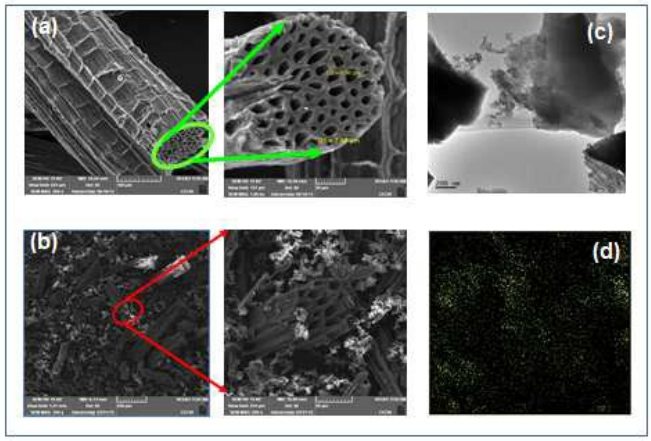

Figure 5. SEM images of (a) activated carbon (b) S-AC and (c) TEM image of S-AC (d) elemental mapping of sulfur

It is well known that electronic conductivity of carbonaceous materials is influenced by their graphitic structures. In the present study the carbon precursor : porogen ratio was fixed at 1:10 be wt.% as large amount of H_3PO_4 could result in serious destruction and rearranging of the layer alignments and reduce the amount of ordered structures, which in turn lower the electronic conductivity of the activated carbon bundles. Moreover, the oxygen groups from the porogen, H_3PO_4, perhaps intrude into the activated carbon bundles inevitably and reduce the electronic conductivity also. Very recently, it has also been demonstrated that 40% of sulfur loading into the carbon matrix was found to be optimal for achieving better electrochemical properties in terms of cycling stability, high-rate capability and specific discharge capacity[45].

In order to understand the electrochemical properties of sulfurized activated carbon (S-AC) electrode, cyclic voltammetry (CV) was first performed at a scan speed of 0.1 mV/s in the potential range of 1.5 V to 3 V as shown in Fig. 6. Typical characteristics of oxidation and reduction curves show the charge –discharge process. The reduction peak that appears around 2.3 V can be assigned to the reduction of open ring of S_8 to long chain lithium polysulfides (Li_2S_x, $4 \leq x \leq 8$). The strong cathodic peak at 2.1 V represents the strong reduction of soluble polysulfide anions to Li_2S_2/Li_2S[27,46]. In the subsequent cycles, (totally 5 cycles) the redox peak currents and potentials under cathodic current, two reductive peaks are observed at 2.0 and 1.80 V that respectively corresponds to redox reaction of high-order polysulfides and Li_2S_2/Li_2S respectively.

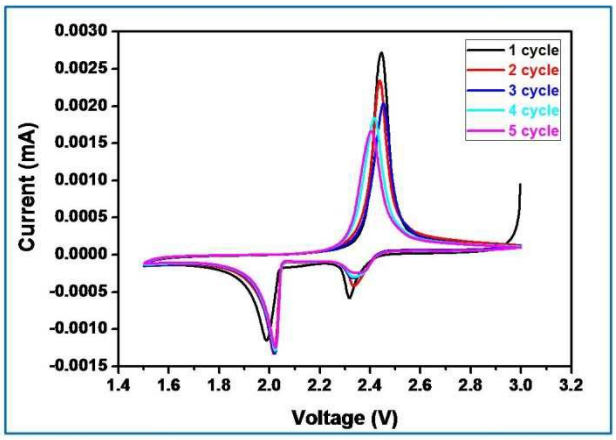

Figure: 6 Cyclic voltammogram of Li-S cell with S-AC electrode. Scanning rate 0.1 mV/sec.

On the other hand, only one oxidation peak was observed at about 2.5 V and is attributed to the oxidation of Li_2S and Li_2S_2 to Li_2S_8. Further no discernible changes could be seen in the redox peak currents and potentials. After two cycles the anodic oxidation of lithium sulfides to polysulfides, the oxidation peak is stabilized which reveals good reactive reversibility and cycling stability of the S-AC cathode.

Figure 7 (a) shows the typical charge-discharge profile of Li-S cell for different current regimes at 25°C. It can be seen from the figure that the charge-discharge patterns remain same even at high current regime. The charge-discharge plateaus at different voltages are already explained elsewhere[5,9]. The two well defined

voltage plateaus at 2.1 and 2.4 V observed in the discharge curve and are in accordance with the two peaks appeared in the CV curves. It is also quite obvious that the activated carbon in the composite electrode is electrochemically inert to the potential region studied and the observed redox curves are attributed only the sulfur present in the composite electrode. The small difference in voltage between the two peaks reflects the asymmetry observed in the oxidation peak in the CV curves.

The cell delivered a discharge capacity of 1050 mAh g^{-1} during its first discharge at 0.05 C-rate which was calculated on the basis of sulfur mass. Generally, pristine sulfur exhibits rapid decrease in discharge capacity with a corresponding Coulombic efficiency of sulfur electrode would be 75% and is attributed to the low utilization and insulating nature of sulfur and volume expansion that arises to the pulverization of sulfur and the high solubility of lithium polysulfides[47]. The reversible Li-S redox reaction occurs through dissimilation process, non- topotactically, in the present study, the volume expansion during charge-discharge cycling is hampered due to the incorporation of sulfur into the AC matrix.

As seen in Figure 7(b) the discharge capacity of Li-S cell with S-AC electrode at lower current rates (0.05 and 0.1C) is seen to decrease very rapidly. It is attributed to the dissolution of polysulfides in the electrolyte and their diffusion and reaction with the lithium metal anode. Surprisingly, at 1C-rate (with short charging and discharging time) the capacity fading was significantly reduced and a stable cycleability was achieved with 99% coulombic efficiency. The better cycleability with appreciable coulombic efficiency is attributed to the slower diffusion of polysulfides to the anode than the total electrochemical reaction time[19,48]. Generally, measurement of coulombic efficiency is widely employed to quantify the shuttle process. According to Moy and co-workers[49], the measured values of coulombic efficiency may vary due to the rate of charge and discharge with a corresponding duration in the shuttle process. For example, the impact on the shuttle process is high for a Li-S cell at low rates. On the other hand, at high rates of charge and discharge, a high value of coulombic efficiency is observed and thus comparison between the high and low rates becomes highly complicated.

It is also noteworthy to mention that most of the Li-S cells cycled at lower C-rate (0.1C) undergo for a capacity fading rapidly[54-56]. The Li-S cell is able to deliver a discharge capacity of 475 mAh $g^{-1}$with a stable cycling.The cells were again cycled at 0.1C-rate. However, the cell suffers from low coulombic efficiency.

We are not able to elucidate the mechanism for this undesirable property which is yet to be understood.

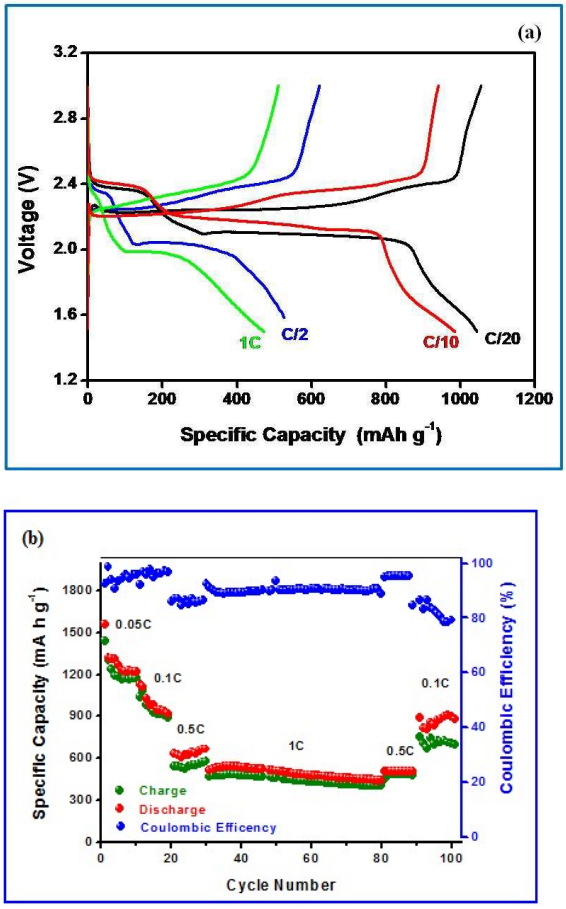

Figure: 7a. Cycling profile of Li-S cell with S-AC electrode (b) Discharge capacity as a function of cycle number

The electrochemical impedance spectroscopy, a non-destructive tool, has always been recognized as one of the most powerful techniques for analyzing the various stages of the complicated mechanism of batteries during the electrochemical reaction. It has been widely employed to characterize Li-S batteries as a whole[53], electrolyte compositions[54] and their influence in the performance[55].

According to Yuan and co-workers[56], EIS can be effectively employed to understand reactions of sulfur cathodes during charge-discharge process. In the frequency domain of EIS, the role of charge transfer resistance, ion diffusion impedance and the influence of Li_2S film in terms of its formation, growth and dissolution can be understood. Figure 8 (a & b) show the Nyquist plots of S-AC/Li cells at different depth of

discharge (DOD) and different depth of charge (DOC). Figure 9 (a) depicts the first discharge-charge profiles of Li-S cell with S-AC electrode at 0.1C-rate and the points where EIS spectra were recorded. The DOD is calculated from the capacity delivered by the cell. According to the shapes, impedance spectra can be broadly classified into two types. Normally the first type appears with a semicircle in the high frequency region followed by a straight line in the low frequency region. The second type shows two depressed semicircles with a long straight line. The semicircle in the middle frequency region shed information on the formation of polysulfides, Li_2S (Li_2S_2) on the S-AC matrix in the cathode. The values of electrolyte resistance, (R_e), charge-transfer resistance (R_{ct}) and film resistance of polysulfides (R_f) obtained from the Nyquist plots for different DOD are displayed in Figure 9 (b).

The value of R_e which represents the ohmic resistance arises due to the contribution from current collector, cell connections and electrolyte resistance[56]. However, the value of R_e is influenced by the electrolyte properties such as chemical composition or viscosity[57]. In the case of Li-S batteries the properties of electrolytes are significantly affected during cycling due to the dissolution of solid products such as sulfur and polysulfides (Li_2S_x with x= 3-8) and are accumulated during cycling which results in increase of electrolyte viscosity and resistance. In the present study, there is small variation in the value of R_e during discharge process and was attributed to the dissolution of polysulfides in the electrolyte[58]. This implies that the concentration of electrolyte is mainly dependent on the state-of-the charge of sulfur electrode at any time which is unfavourable for the formation of solid electrolyte interface (SEI) layer on the anode. Obviously, this affects the cycling efficiency of Li-S cells. It can be seen from Figure 9 (b) that value of R_e was found to be higher for 17% DOD which indicates the presence of maximum amount of polysulfides (concentrations) at the end of first plateau of the discharge. Upon the complete reduction of the polysulfides to Li_2S_2, the value of R_e is reduced and almost reaches its initial value. The value of R_f also varies with the level of DOD and finally reaches a maximum when the DOD was 100%. The formed Li_2S_2 or Li_2S film causes Warburg impedance due to their diffusion within the cathode. The angle of Warburg impedance is close to 45° which implies that the surface of the sulfur cathode at 0.5% and 21%of DOD. At higher DOD and cycles the angle of the Warburg diffusion decreases due to the slow ion diffusion into the sulfur cathode due to increase in concentration of lithium polysulfides at the cathode-electrolyte interface[59].

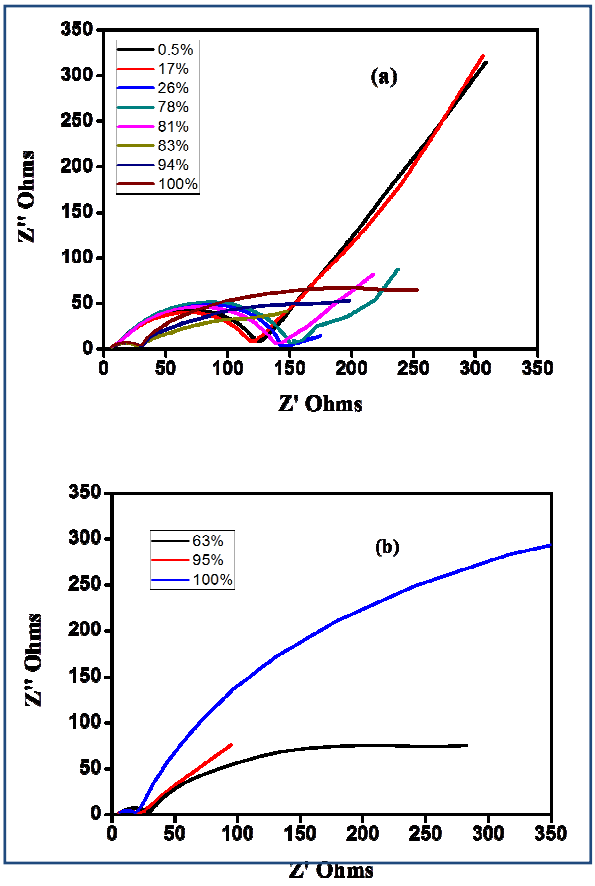

Figure 8. Nyquist plots (a) for different DOD (b) for different DOC.

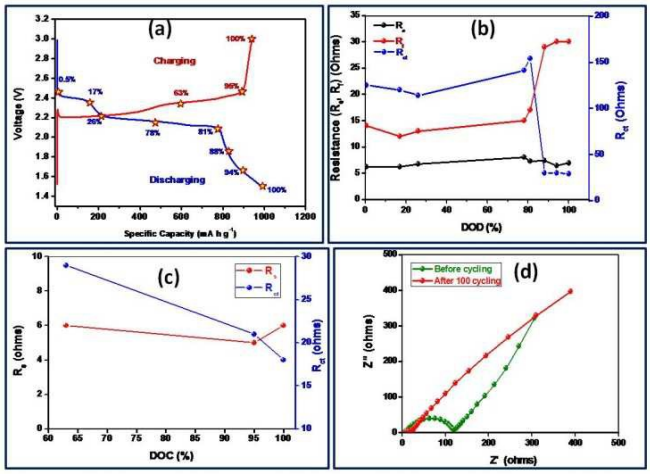

Figure 9 (a) The cycling profile with various DOD and DOC (b) The variation of R_e, R_f and R_{ct} for various DOD and (c) DOC (d) The EIS spectra of Li-S cell before and after cycling.

On the other hand, during discharge a dramatic reduction in the value of R_{ct} has been observed. This causes due to the changes in composition and

morphology occurring in the cathode. The dissolution and reaction of sulfur, subsequently reduces the sulfur content in the cathode and this makes a porous structure with high surface area. This in turn increases the conductivity. In a similar way, the variations of R_e, R_f and R_{ct} for difference depth of charge (DOC) are displayed in Figure 9 (c). Contrary to the first discharge process, maximum concentration of polysulfides is seen when DOC was 63%. i.e. during the second plateau region indicating the complete reaction of Li_2S to S_8[59]. The EIS of Li-S cell before and after 100 cycles is shown in Figure 9 (d). After 100 cycles, the resistance of the Li-S cell with S-AC electrode is greatly reduced (approximately 25 ohm). Unlike the usual increase of those with conventional sulfur electrodes, the sulfurized activated carbon electrode exhibits lower resistance value which is attributed to the prevention of aggregation of Li_2S on the cathode[60,61]. Thus sulfurized activated carbon electrode exhibits a low resistance value and this appreciable performance qualifies it as a promising electrode material for Li-S batteries.

Conclusions

Activated carbon was derived by the pyrolysis of sisal fiber with phosphoric acid as porogen. The elemental sulfur was successfully impregnated in to the AC matrix in order to prevent the pulverization of sulfur particles and to enhance their conductivity. The Li-S cells with S-AC electrode delivered although a discharge capacity of 1050 and 1000 mAh g^{-1} at 0.05 and 0.1 C-rate respectively. However, the cycleability and Coloumbic efficiency of the Li-S cell were found to be inferior to 1C-rate. This better cycleability at 1C-rate was attributed to the slower diffusion of polysulfides to the anode than the total electrochemical reaction time. The study demonstrates that the S-AC electrode with appreciable electrochemical properties may be suitable for cost-effective lithium-sulfur batteries.

Acknowledgements

One of the authors M. Raja gratefully acknowledges AcSIR, CSIR-CECRI, Karakudi, 630 006.

Address

*Electrochemical Power Sources Division, CSIR – Central Electrochemical Research Institute, Karaikudi, 630 006, India.
E-mail: arulmanuel@gmail.com; amstephan@cecri.res.in
Present address; M G. University, Kottayam 686560
E-mail:anguluxmi@gmail.com
Fax: +91 4565 227779 Phone: +91 4565 241426

References

1 P.G. Bruce, S. A. Freunberger, L.J. Hardwick, J.M. Tarascon, *Nat. Mater*., 2012, **11**, 19-30.
2 S. Evers, L.F. Nazar, Acc. Chem. Res., 2013, **46**, 1135-1143.
3 M. Armand, J.-M. Tarascon, *Nature* , 2008, **451**, 652-657.
4 J. Hassoun, B. Scrosati, *Angew. Chem. Int. Edn*., 2010, **49**, 2371-2374.
5 X. Ji, K. T. Lee, L.F. Nazar, *Nat. Mater.,* 2009, **8**, 500-506.
6 A. Manthiram, Y. Fu, Y.S.Su, *Acc. Chem., Res*., 2013, **46**, 1125-1134.
7 M.K.Song, E.J. Cairns, Y. Zhang, *Nanoscale*, 2013, **5**, 2186-2204.
8 Y. Yang, G. Y. Zheng, N. Cui, *Chem. Soc. Rev*., 2013, **42**, 3018-3032.
9 Y.X.Yin, S.Xin, Y.G Guo, L.J.Wan, *Ang.Chem. Int.Edn.*, 2013, **52**, 13186-13200.
10 D. Herbert, J. Ulam, *US Patent*, 1962, 3, 043,896
11 D. Aurbach, E. Pollak, R. Elazari, G. Salitra, C.S.Kelley, Affinito, *J. Electrochem. Soc.,* 2009, **156**, A694-A702.
12 Z. Lin, Z. Liu, W. Fu, N. J. Dudney, C. Liang, *Adv. Funct. Mater*., 2013, **23**, 1064-1069.
13 A. Gorkovento, *US Patent, No*.6, 210, 831, B1. 2001.
14 M.S. Song, S.C. Han, H.S. Kim, J. H. Kim, K. T. Kim, Y. M. Kang, H. J. Ahn, S. X. Dou, J. Y. Lee, *J. Electrochem. Soc*., 2004, **51**, A791-A795.
15 N. Tachikawa, Y. Yamauchi, E. Takashima, J. W. Park, K. Dokko, M. Watanabe, *Chem. Comm*., 2011, **47**, 8157-8159.
16 Y. Fu, Y. Su, A. Manthiram, *ACS Appl.Mater.& Interface,* 2012, **4**, 6046-6052
17 K. Jin, X. Zhou, L. Zhang, X. Xin, G.Wang, Z. Lin, *J. Phys. Chem C*, 2013, **117**, 21112-21119.
18 Y. Yang, G. Yu, J.J. Cha, H. Wu, M. Vosguentchian, Y. Yao, Z. Bao, Y. Cui, *ACS Nano*, 2011, **5**, 9187-9193.
19 J. Bruckner, S. Thieme, H. T. Grossmann, S. Dorfler, H. Althues, S. Kaskel, *J. Power Sources*, 2014, **268** , 82-87.
20 H. Ye, Y.X. Yin, S. Xin, Y. G. Guo, *J. Mater. Chem. A* , 2013, **1,** 6602-6608.
21 M. Barghamadi, A.S. Best, A.I.Bhatt, A. F. Hollenkamp, M. Musameh, R. J. Rees, T. Ruther, *Energy & Environ. Sci.,* 2014, **7**, 3902-3920.
22 W. Xing, J.S. Xue, J. R. Dahn, *J. Electrochem. Soc.,* 1996, **143**, 3046-3052.
23 G. T. K. Fey, D.C. Lee, Y. Y. Lin, T. Prem Kumar, *Synth. Met.,* 2003, **139**, 71-80.
24 J.C. Arrebola, A. Caballero, L. Hernan, J. Morales,

J. Electrochem. Soc., 2001, **157,** A791-A797.
25 A. Manuel Stephan, T. Prem Kumar, R. Ramesh, S. Thomas, J.K. Jeong, K.S. Nahm ,*Mater. Sci. Engg. A*, 2006, **430**,132-137..
26 V. Subramanian, A. Manuel Stephan, S. Thomas, K.S. Nahm, W. Bei, *J. Phys. Chem. C,* 2007, **111**, 7527-7531.
27 N. Moreno, A. Caballero, L. Hernan, J. Morales, *Carbon* , 2014, **70**, 241-248.
28 Q. Wang, J. Jin, X. Wu, G. Ma, J. Yang , Z. Wen, Phys. Chem. Chem. Phys. 2014, 16, 21225
29 G. Ma, Z. Wen, M.n Wu, C. Shen, Q. Wang, J. Jin, X. Wu, Chem Commun, 2014, 50, 14209
30 G. Ma, Z. Wen, Q. Wang, C. Shen, J. Jin, X. Wu, J. Mater. Chem. A, 2014, 2, 19355
31 Q. Wang, Z. Wen, J. Jin, J. Guo, X. Huang, J. Yanga, C. Chen, Chem. Commun. 2015, :DOI: 10.1039/c5cc08279j
32 N. Angulakhsmi, A. Manuel Stephan, *Electrochim. Acta*, 2014, **67**, 167-172.
33 A. Ahmadpour, D.D. Do, Carbon, 1997, **35**, 1723-1732.
34 X. Lu, J. Jiang, K. Sun, X. Xie, *Bull. Korean chem. Soc.,* 2014, **35**, 103-110.
35 Y. J. Hwang, S. K. Jeong, K. S. Nahm, J. S. Shin, A. Manuel Stephan, *J. Phys.&Chem. Solids*, 2007, **68**, 182-188.
36 F. Caturla, M. Molina-Sabio, F. Rodriguez-Reinoso, *Carbon*, 1991, **29**, 999-1007.
37 M. Molina-Sabio, F. Rodriguez-Reinoso, F. Caturla, M. J. Selles, *Carbon*, 1995, **33**, 1105-1113.
38 A. Ahmadpour, D.D. Do, *Carbon*, 1996, **34**, 471-479.
39 Z. Hu, M. P. Srinivasan, Y. Ni, *Carbon,* 2001, **39**, 877-886.
40 C. Moreno-Castilla, F. Carrasco-Marin, M. V. Lopez-Ramon, M. A. Alvarez-Merino, *Carbon,* 2001, **39**, 1415-1420.
41 H. Marsh, D. S. Yan, *Carbon*, 1984, **22**, 603-611.
42 Y.Li, J. S. Xue, J. R. Dahn, Carbon, 1996, **34**, 193-200.
43 Y. S. Su, A. Manthiram, *Electrochim.Acta*, 2012, **77**, 272-278.
44 G. Katagiri, H. Ishida, A. Ishitani, *Carbon,* 1998, **26**, 565-571.
45 H. Ye, Y. X. Yin, S. Xin, Y. G. Guo, *J. Mater. Chem. A,* 2013, **1**, 6602-6608..
46 G. Xu, B. Ding, L. Shen, P. Nie, J. Han, X. Zhang, *J. Mater. Chem. A,* 2013, **1**, 4490-4496.
47 N. Jayaprakash, J. Shen, S. S. Moganty, A. Corona, L. A. Archer, *Angew. Chem.Int. Ed.,* 2011, **50**, 5904-5908.
48 Y. V. Mikhaylik, J. R. Akridge, *J. Electrochem. Soc.,* 2004, **11**, A1969-A1976.
49 D. Moy, A. Manthiram, S. R. Narayanan, *J. Electrochem. Soc.* 2015, **162**, A1-A7.
50 I. Bauer, S. Thieme, J. Brucker, H. Althus, S. Kaskel, *J. Power Sources* 2014, **251**, 417-422.
51 Z. Ma, X. Huang, Q. Jiang, J. Huo, S. Wang, *Electrochim. Acta* 2015 accepted manuscript.
52 J. Guo, J. Zhang, F. Jiang, S. Zhao, Q. Su, G. Du, *Electrochim. Acta* 2015 accepted manuscript.
53 H. Yamin, E. Peled, *J. Power Sources*, 1983, **9,** 281-287.
54 H. S. Rya, H. J. Ahn, K. W. Kim, T. H. Nam, J. V. Kim, G. B. Cho, *J. Power Sources*, 2006,**163**, 201-206.
55 S. S. Zhang, D. T. Tran, *Electrochim. Acta,* 2013, **114**, 296
56 L. Yuan, X. Qui, W. Zhu, *J. Power Sources*, 2009, **189**, 27
57 V. S. Kolosnitsyn, E. V. Kuzmina, E. V. Karaseva, S. E. Mochalov, *Russian J. Electrochem*., 2011, **47**, 793-798.
58 C. Barchasz, J. C. Lepretre, F. Alloin, S. Patoux, *J. Power Sources*, 2012, **199**, 322-330.
59 N. A. Cans, S. Wolf, N. Wanger, K. A. Friedrich, *J. Power Sources*, 2013, **226**, 313-319.
60 N. A. Cans, K. Hirose, B. Pascucci, N. Wanger, K. A. Friedrich, R. Hiesgen, *Electrochimi. Acta*, 2013, **97**, 42-51.
61 Y. J. Choi, Y. D. Chung, C. Y. Baek, K. W. Kim, H. J. Ahn, *J. Power Sources*, 2008, **184**, 548-552.

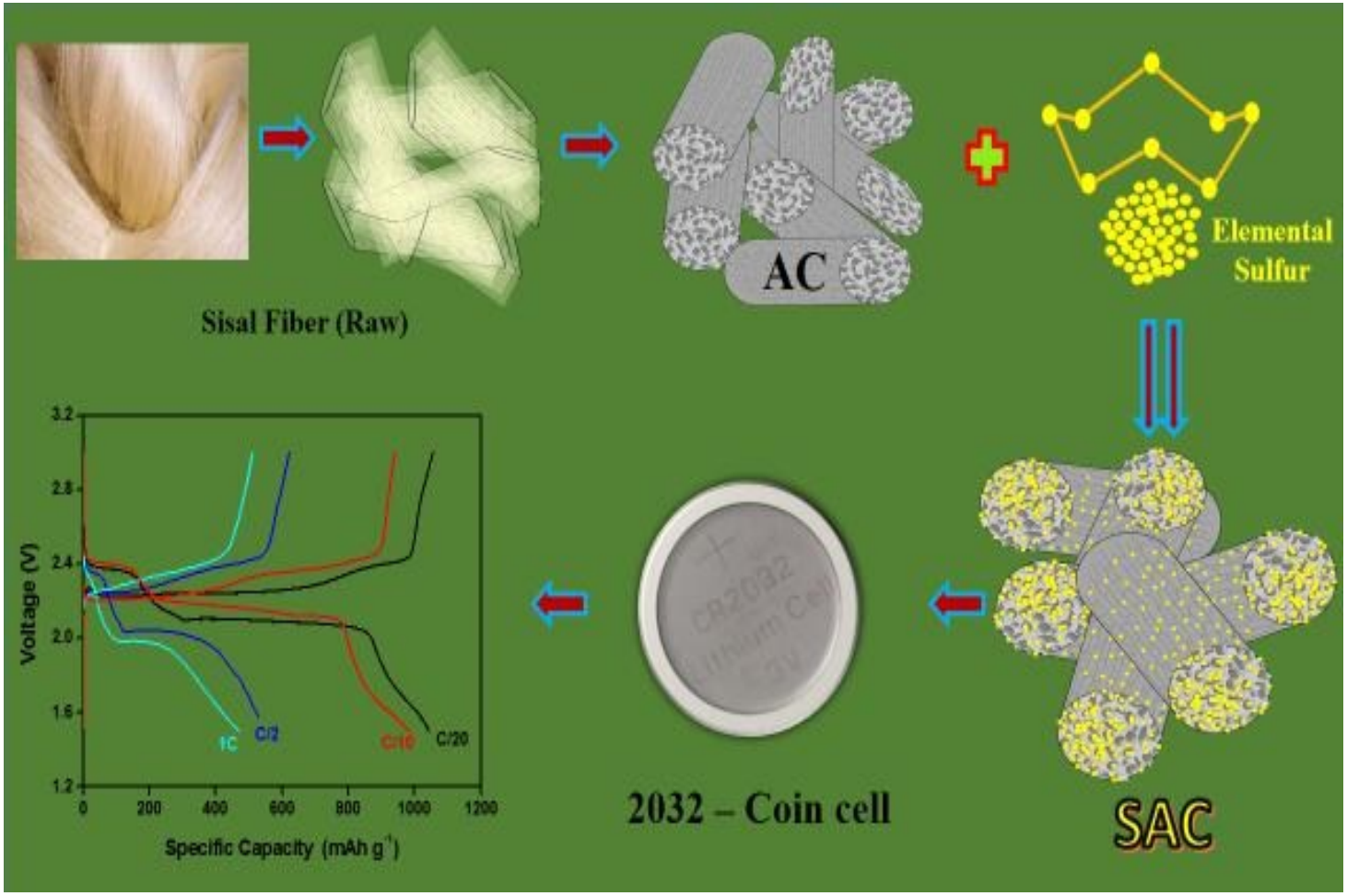

Graphical Abstract

Sisal-derived activated carbons for cost-effective lithium-sulfur batteries

M. Raja, N. Angulakshmi, A. Manuel Stephan*